# Uncharacterized bacterial structures revealed by electron cryotomography

Megan J. Dobro[1], Catherine M. Oikonomou[2], Aidan Piper[1], John Cohen[1], Kylie Guo[2], Taylor Jensen[2], Jahan Tadayon[2], Joseph Donermeyer[2], Yeram Park[2], Benjamin A. Solis[3], Andreas Kjær[4], Andrew I. Jewett[2], Alasdair W. McDowall[2], Songye Chen[2], Yi-Wei Chang[2], Jian Shi[5], Poorna Subramanian[2], Cristina V. Iancu[6], Zhuo Li[7], Ariane Briegel[8], Elitza I. Tocheva[9], Martin Pilhofer[10], Grant J. Jensen[2,11,*]

1 Hampshire College, 893 West St., Amherst, MA 01002
2 California Institute of Technology, 1200 E. California Blvd., Pasadena, CA 91125
3 University at Albany, SUNY, 135 Western Avenue, Albany, NY. 12203
4 University of Southern Denmark, Campusvej 55, 5230 Odense M, Denmark
5 National University of Singapore, 21 Lower Kent Ridge Road, Singapore 119077
6 Rosalind Franklin University of Medicine and Science, 3333 Green Bay Rd., North Chicago, IL 60064
7 City of Hope, 1500 E. Duarte Road, Duarte, CA 91010
8 Leiden University, Sylvius Laboratories, Sylviusweg 72, 2333 BE, Leiden, Netherlands
9 University of Montreal, C.P. 6128, succursale Centre-ville, Montreal, Quebec, Canada
10 ETH Zurich, Otto-Stern-Weg 5, 8093 Zurich, Switzerland
11 Howard Hughes Medical Institute, 1200 E. California Blvd., Pasadena, CA 91125
* To whom correspondence should be addressed. Tel: (626) 395-8827. Email: jensen@caltech.edu

Running title: ECT of novel bacterial structures

Keywords: bacteria, electron cryotomography, cryo-EM, bacterial ultrastructure, uncharacterized structures

## SUMMARY STATEMENT

Here we present a survey of previously uncharacterized structures we have observed in bacterial cells by electron cryotomography, in the hopes of spurring their identification and study.


## ABSTRACT

Electron cryotomography (ECT) can reveal the native structure and arrangement of macromolecular complexes inside intact cells. This technique has greatly advanced our understanding of the ultrastructure of bacterial cells. Rather than undifferentiated bags of enzymes, we now view bacteria as structurally complex assemblies of macromolecular machines. To date, our group has applied ECT to nearly 90 different bacterial species, collecting more than 15,000 cryotomograms. In addition to known structures, we have observed several, to our knowledge, uncharacterized features in these tomograms. Some are completely novel structures; others expand the features or species range of known structure types. Here we present a survey of these uncharacterized bacterial structures in the hopes of accelerating their identification and study, and furthering our understanding of the structural complexity of bacterial cells.


## IMPORTANCE

Bacteria are more structurally complex than is commonly appreciated and we present here a number of interesting structures that will initiate new lines of research investigating their identities and roles.

## INTRODUCTION

The history of cell biology has been punctuated by advances in imaging technology. In particular, the development of electron microscopy in the 1930s produced a wealth of new information about the ultrastructure of cells (Ruska, 1987). For the first time, the structure of cell envelopes, internal organelles, cytoskeletal filaments and even large macromolecular complexes like ribosomes became visible. A further advance came in the 1980s and 1990s with the development of electron cryotomography (ECT) (Koster *et al.*, 1997), which allows small cells to be imaged intact in 3D in a near-native, "frozen-hydrated" state to "macromolecular" (~5 nm) resolution, without the limitations and artifacts of more traditional specimen preparation methods (Pilhofer *et al.*, 2010).

ECT has helped reveal the previously unappreciated complexity of "simple" bacterial cells. Our group has been using ECT to study bacteria for more than a decade, generating more than 15,000 tomograms of 88 different species. These tomograms have revealed new insights into, among other things, the bacterial cytoskeleton (Komeili *et al.*, 2006, Li *et al.*, 2007, Pilhofer *et al.*, 2011, Swulius & Jensen, 2012), cell wall architecture (Gan *et al.*, 2008, Beeby *et al.*, 2013), morphogenesis (Ebersbach *et al.*, 2008), metabolism (Iancu *et al.*, 2007), motility (Murphy *et al.*, 2006, Chen *et al.*, 2011, Abrusci *et al.*, 2013, Chang *et al.*, 2016), chemotaxis (Briegel *et al.*, 2012), sporulation (Tocheva *et al.*, 2011), cell-cell interactions (Basler *et al.*, 2012), and phage infection (Guerrero-Ferreira *et al.*, 2011) (for a summary with more references from our and others' work, see (Oikonomou & Jensen, 2016)).

A major hurdle in such studies is identifying the novel structures observed in tomograms. In some cases, we have identified structures by perturbing the abundance (either by knockout or overexpression) of candidate proteins (Ingerson-Mahar *et al.*, 2010). In others, we have used correlated light and electron microscopy (CLEM) to locate tagged proteins of interest (Briegel *et al.*, 2008, Chang *et al.*, 2014). In one striking example, we observed 12- and 15-nm wide tubes in our tomograms of *Vibrio cholerae* cells. Ultimately, in collaboration with John Mekalanos' group, we identified them as type VI secretion systems (T6SS), which immediately led to the insight that the bacterial T6SS functions as a phage-tail-like, contractile molecular dagger (Basler *et al.*, 2012).

Many other novel structures we have observed, though, remain unidentified. In some cases, we have published papers describing the novel structures seen in a particular species (e.g. (Murphy *et al.*, 2008, Muller *et al.*, 2014)), but many have never been published. We therefore conducted a visual survey of the tomograms collected by our group, curated in the Caltech Tomography Database (Ding *et al.*, 2015), as of 2015 and present here a catalog of previously undescribed bacterial structures. Some structures are, to our knowledge, completely novel; others belong to known types but present additional features or an expanded species range. We hope that sharing these images will help spur their identification and study, contributing to our expanding understanding of bacterial cell biology. In addition, we look forward to a future in which custom microbes are designed for diverse medical and industrial purposes; an expanded "parts list" of structures to be repurposed will aid in this effort.

## RESULTS AND DISCUSSION

We performed a visual inspection of approximately 15,000 tomograms of intact, frozen-hydrated cells belonging to 88 species and identified what we believed to be novel structures. A summary of the results of this survey is shown in Supplementary Table 1, with features observed, species range, and frequency listed for each structure type. For full tomographic (3D) views of each feature, please see the accompanying supplementary movies at the following link: https://figshare.com/s/782461843c3150d27cfa. The figures can also be viewed in virtual reality: https://play.google.com/store/apps/details?id=com.BishopVisual.Mk2&rdid=com.BishopVisual.Mk2.

### Extracellular structures

#### *External appendages*

*Prosthecobacter debontii* is a bacterial species from the poorly studied phylum *Verrucomicrobia*. Each vibroid *P. debontii* cell possesses an appendage (prostheca), similar to the stalk of *Caulobacter crescentus* (Staley *et al.*, 1976). In several tomograms of *P. debontii,* we observed novel extracellular appendages along the prosthecae, apparently attached to the cell membrane. Individual cells displayed up to 30 such appendages, which exhibited consistent size (~20 nm wide and ~50 nm long) and shape (Figure 1A). Subtomogram averaging of 105 particles revealed a distinctive structure: extending outward from the cell membrane, five legs were attached to a disc, which in turn connected to a smaller disc and a long neck region (Figure 1B,C). Individual particles showed that the structure culminated in two antenna-like filaments, which were likely lost in the average due to conformational variability. The appendages were observed in multiple cultures of the strain. While it remains unclear whether they originated

intra- or extracellularly, no free-floating appendages were ever observed in the extracellular space. They may represent novel bacterial attachment organelles or appendages for nutrient acquisition, which has been proposed for a similar structure— the *Caulobacter* stalk. Under phosphate limited conditions, *Caulobacter* grew elongated stalks (Gonin *et al*., 2000). This increase in cell surface area with respect to cell volume was proposed to allow increased phosphate uptake (Wagner *et al*., 2006). However, the presence of diffusion barriers challenges this view (Schlimpert *et al*., 2012). The appendages could also be a novel secretion system (though we might expect a cell envelope spanning complex) or a novel bacteriophage (though there is a notable lack of a capsid-like density).

We observed a different novel extracellular appendage in tomograms of cell poles of *Azospirillum brasilense,* a plant growth-promoting bacterium of the *α-Proteobacteria* class with a curved rod morphology. Thin hooks were seen extending out from the cell surface (Figure 2). Individual cells exhibited dozens of hooks, each ~3 nm wide and ~75 nm long, associated with the outer membrane. The cells are large and most tomograms only included the cell pole region, so while hooks were only observed at the pole region, they may also occur elsewhere on the cell. Hooks were seen in >90% of wild-type cells as well as in a strain in which the operon encoding the Che1 chemotaxis system was deleted. They were seen in ~50 % of cells in which the Che4 chemotaxis system operon was deleted, and none were seen in cells lacking both the Che1 and Che4 operons. *A. brasilense* is a well-studied plant growth-promoting bacterium. Cells attach to plant roots through a two-step process (De Troch & Vanderleyden, 1996): a rapid, reversible adsorption thought to be mediated by the polar flagellum; and a slow, irreversible anchoring, thought to be mediated by an as-yet unidentified surface polysaccharide (Steenhoudt &

143 Vanderleyden, 2000). A recent study reported that mutants in components of the Che4
144 chemotaxis system are defective in this root colonization (Mukherjee *et al.*, 2016). *A. brasilense*
145 cells also attach to conspecifics in the presence of elevated oxygen levels (Bible *et al.*, 2015).
146 Interestingly, it has been shown that mutants in components of the Che1 chemotaxis system form
147 such attachments more rapidly than wild-type cells (Bible *et al.*, 2012). The hooks we observed
148 are vaguely reminiscent of the grappling hook-like structures that an archaeal species uses to
149 anchor itself in biofilms (Moissl *et al.*, 2005), though those hooks were longer fibers with barbs.
150 Those archaeal cells demonstrated very strong adhesion to a variety of surfaces as well as to each
151 other. It is therefore tempting to speculate that the hooks shown here play a similar role in
152 adhesion, either to other *A. brasilense* cells or to plant roots.
153
154 In cells of strain JT5 (a rod-shaped bacterium isolated from termite gut and related to the
155 *Dysgonomonas* genus), we observed abundant fimbriae concentrated at the cell poles (Figure 3).
156 Fimbrae were also observed at the cell body but were much more concentrated at the cell poles.
157 They were present in cells grown on cellulose or xylan, as well as in a condition inducing
158 starvation. Their width (~4 nm), apparent flexibility, density on the cell envelope, and
159 inhomogeneous distribution around the cell is consistent with curli, functional amyloids secreted
160 by the type VIII secretion system that are involved in adhesion (Epstein *et al.*, 2009; Van Gerven
161 *et al.*, 2015). Curli systems are relatively divergent at the sequence level, but are remarkably
162 widespread phylogenetically, and the genes were reported to be present in Bacteroidetes (the
163 phylum containing *Dysgonomonas*) (Dueholm *et al.*, 2012). The appendages we observed in
164 strain JT5 may therefore play a role in adhesion in the environment of the termite gut.
165

## Intracellular structures

***"Nanospheres"***

In two *Vibrio cholerae* cells (one from a C6706 lacZ⁻ strain (Cameron *et al.*, 2008), and one from a ΔctxA ΔtcpB strain (Chang *et al.*, 2016)) we observed clusters of "nanospheres" – hollow granules with thick walls (Figure 4). The diameter of the nanospheres ranged from ~18-37 nm, and the walls were ~4-10 nm thick. They were pleomorphic: most were roughly spherical, but some were oblong or comma shaped. Each cluster contained about two dozen nanospheres. The clusters were observed at the cell periphery, near the inner membrane (although the clusters were large enough to extend to the center of the cell), and were always observed in close proximity to a filament array structure (discussed below).

***Filaments, bundles, arrays, chains and meshes***

One of the strengths of ECT imaging is its power to resolve cytoskeletal elements in small bacterial cells. In addition to those we have already identified, we observed many novel filamentous structures in tomograms, including filament arrays, bundles, chains and meshes (Figure 5). In *Hyphomonas neptunium*, we observed long helical filament bundles in the prosthecae that connect dividing cells (Figure 5A). The helix width was 9.5 ± 1.5 nm, the spacing between cross-densities 6.0 ± 0.3 nm, and the helical pitch ~26°. *H. neptunium* divides by asymmetric budding (Weiner *et al.*, 2000) and the genome of the parent cell is passed to the daughter cell through the narrow prostheca connecting the two cells (Zerfas *et al.*, 1997). We observed that the helical structure was straightened in cells treated with ethidium bromide (an intercalator known to unwind DNA (Pommier *et al.*, 1987)) (Figure 5B). We therefore propose

188 that the helix is composed of supercoiled DNA, with each visible filament a DNA duplex
189 connected to adjacent duplexes by cross-densities formed by an unidentified protein.
190
191 In *Helicobacter pylori* cells we observed extensive filament bundles. In one cell in an early
192 stage of lysis, such bundles were observed throughout most of the cell (Figure 5C). In *V.*
193 *cholerae* we observed filament arrays resembling a honeycombed mesh (Figure 5D). These
194 arrays varied in length, but were usually fairly short (~100 nm in length and width), like the
195 example shown in Figure 5E. This is the structure we observed near the nanosphere clusters.
196 Filament arrays exhibited different morphologies in other species. *Thiomonas intermedia* cells
197 contained untwisted arrays ~48 nm thick, ~30 nm wide (Figure 5F). In addition to the prosthecal
198 helix described above, *H. neptunium* cells also contained a bundle of twisting filaments laddered
199 by cross-densities (Figure 5G). These bundles were ~40 nm thick and ~75 nm wide. In a
200 *Hylemonella gracilis* cell we observed a helical bundle of filaments that varied in width and
201 could be related to the nucleoid (Figure 5H). In *Halothiobacillus neapolitanus* c2 cells grown in
202 limited $CO_2$ for several hours we observed linear filament arrays with prominent cross-densities
203 spaced 7 ± 0.8 nm apart (Figure 5I). *Mycobacterium smegmatis* displayed straight arrays ~80 nm
204 thick and wide, comprising segments of pitched filaments (Figure 5J). Filament arrays were also
205 seen in multiple species of *Prosthecobacter*: *P. vanneervenii* contained linear chains (Figure 5K)
206 and one *P. debontii* cell contained a straight array similar to those observed in *T. intermedia*
207 (Figure 5L) as well as mesh-like arrays spanning the width of the prostheca (Figure 5M).
208
209 In starving *Campylobacter jejuni* cells, we observed regular filament arrays (Figure 5N). When
210 subjected to environmental or cellular stress some bacteria, including *Escherichia coli*, have been

shown to reorganize their DNA into protective crystalline arrays (Wolf *et al.*, 1999). Since then, additional nucleoid associated proteins have been identified that organize DNA into higher order structures in stationary phase or stress conditions (Teramoto *et al.*, 2010, Lim *et al.*, 2013). The structures we observed in *C. jejuni* resemble those seen in *E. coli* cells overexpressing the protective DNA binding protein Dps (Wolf *et al.*, 1999) and may therefore represent such a nucleoprotein array.

Several other proteins have been shown to copolymerize with DNA into filaments for various functions, including RecA (homologous recombination) (Egelman & Stasiak, 1986) and MuB from bacteriophage Mu (DNA transposition) (Mizuno *et al.*, 2013). The width of such filaments *in vitro* (~10 nm) is similar to widths we observed in cells; it is possible that some of the structures in Figure 5 represent these DNA-related processes. Other bacterial proteins form filaments to regulate their function, and it has been suggested that this property may have been coopted in the evolution of the cytoskeleton (Barry & Gitai, 2011). We previously observed such filaments of CTP synthase in tomograms of *C. crescentus* cells (Ingerson-Mahar *et al.*, 2010). Another protein, alcohol dehydrogenase, forms plaited filaments ~10 nm wide, called spirosomes, in many bacteria capable of anaerobic metabolism (Matayoshi *et al.*, 1989, Laurenceau *et al.*, 2015). It is possible that some of the filament arrays and chains we observed in tomograms may be filaments formed by these or other, yet uncharacterized, proteins.

In addition to filament arrays and bundles, we observed individual or paired filaments in nearly every species imaged. Examples are shown in Figure 6. (Note that due to their ubiquity, statistics are not included in Supplementary Table 1.) Filaments were seen with various

234 orientations in the cytoplasm (Figure 6A-C), as well as running alongside the membrane (Figure
235 6D-E). Consistent with our previous work (Swulius *et al.*, 2011), we did not observe any
236 filaments immediately adjacent to the membrane as predicted by some studies of MreB (e.g.
237 (Jones *et al.*, 2001, Shih *et al.*, 2003)). (Note that we did observe filaments corresponding to the
238 known types of MamK (Komeili *et al.*, 2006, Scheffel *et al.*, 2006), FtsZ (Li *et al.*, 2007,
239 Szwedziak *et al.*, 2014), and bactofilins (Kuhn *et al.*, 2010) but we do not show them here since
240 they have already been characterized.) Paired filaments have been shown to function in plasmid
241 segregation, so it is possible that some paired filaments we observed were such ParM or TubZ
242 structures (Aylett *et al.*, 2010, Bharat *et al.*, 2015).
243
244 ***Tubes***
245 In addition to the known types of tubes we have reported earlier, such as bacterial microtubules
246 (Pilhofer *et al.*, 2011) and type VI secretion systems (Basler *et al.*, 2012)), we observed several
247 novel tubular structures in bacterial cells (Figure 7). In *Thiomicrospira crunogena* we found
248 large tubes (18.6 ± 1.8 nm diameter) containing eight outer protofilaments surrounding a central
249 protofilament (Figure 7A). *H. neapolitanus* c2 cells also contained large tubes (16.7 ± 0.7 nm
250 diameter) with a central filament (Figure 7B). In several other species, we observed hollow tubes
251 of varying dimensions: 8.9 ± 0.3 nm diameter in *Bdellovibrio bacteriovorus* (Figure 7C), 14.3 ±
252 1.7 nm in *T. intermedia* (Figure 7D), and 8.3 ± 0.5 nm in *H. neptunium* (Figure 7E). *H.*
253 *neptunium* cells also contained many rings of similar diameter. In fact, we observed rings in
254 many species, which could be assembly or disassembly intermediates of tubes.
255

In addition to isolated rings, in one case we observed an organized array of rings. One slightly lysed (a condition that flattens the cell and increases image quality) *H. pylori* cell contained a striking array of about two dozen evenly spaced rings near the cytoplasmic membrane (Figure 7F). Each ring was ~6 nm in diameter and ~20 nm (center-to-center distance) from its neighbors in the square lattice.

***Vesicles***

In contrast to eukaryotic cells, relatively little is known about membrane remodeling in bacteria. Compartmentalized cells in the Planctomycetes-Verrucomicrobia-Chlamydiae (PVC) superphylum have been shown to contain homologs of eukaryotic membrane trafficking proteins (Santarella-Mellwig *et al.*, 2010) and exhibit endocytosis-like protein uptake (Lonhienne *et al.*, 2010). An additional potential membrane-remodeling system based on FtsZ homologues is more widespread across bacteria, but its function remains unknown (Makarova & Koonin, 2010).

Despite this limited evidence for membrane remodeling in bacteria, we observed intracellular vesicles in nearly every species imaged. They exhibited various sizes, shapes, membrane layers, and contents, and were frequently found near the cytoplasmic membrane. Figure 8 shows examples of round and horseshoe-shaped vesicles. Round vesicles were found in nearly every species imaged, and therefore no statistics for them are compiled in Supplementary Table 1. Most round vesicles were empty (density similar to background; e.g. Figure 8A-C). One of these vesicles, observed in a lysed cell (improving clarity by reducing cytoplasmic crowding), exhibited regularly spaced protein densities around its exterior (Figure 8C). Others were at least partially filled with denser material (e.g. Figure 8D-F). In two *Myxococcus xanthus* cells

overexpressing a fluorescent fusion of a periplasmic protein (PilP-sfGFP), we observed round vesicles containing a dense amorphous core (Figure 8F). These could be a novel form of membrane-bound inclusion bodies, perhaps packaged from the periplasm. In eight species, we observed horseshoe-shaped vesicles (Figure 8G-H).

Flattened vesicles (Figure 9A-F) were less common than round vesicles, and were usually observed near membranes or wrapping around storage granules (Figure 9E), suggesting a possible functional relationship. Flattened vesicles were usually empty. One *T. intermedia* cell contained a stack of flattened vesicles (Figure 9A). Flattened vesicles were particularly prevalent in *C. crescentus* cells (Figure 9B-E). *P. debontii* cells contained flattened vesicles that neither ran along the membrane nor wrapped around granules (Figure 9F). Since the lowest energy shape of a liposome is a sphere, it is likely that the vesicles were flattened by cytoplasmic pressure or some other constraint such as associated protein.

Many cells contained nested vesicles, with diverse sizes and shapes, as well as subcellular locations (Figure 9G-L). In some nested vesicles, densities were observed bridging the inner and outer membranes (Figures 8A and 9G-H). Cells of strain JT5 exhibited multiple nested vesicles of uniform shape and size (Figure 9L).

We also observed periplasmic vesicles in many species (Figure 10). They were typically empty and exhibited great variability in size, shape, and abundance. In some cases, they were even seen to form branching networks (Figure 10A). As with cytoplasmic vesicles, they were most

abundant in cells showing signs of stress (rupture of inner or outer membrane, separation of inner and outer membrane, lysis, or membrane blebbing).

## Conclusions

Here we present the results of a survey of, to our knowledge, uncharacterized bacterial structures that we have observed in our work over the last 10+ years. We hope that further study will identify them and their functions. Already, they signal the wealth of complexity still to be discovered in bacterial cells.

## MATERIALS and METHODS

*Strains and growth*

Unless otherwise noted, bacterial strains were wild-type and grown in species-standard medium and conditions to mid-log or early stationary phase. *Azospirillum brasilense* cultures were switched to nitrogen-free medium for ~16 hours prior to imaging to induce nitrogen fixation and digestion of storage granules that decrease image quality. Predatory *Bdellovibrio bacteriovorus* cells were co-cultured with *Vibrio cholerae* strain MKW1383. *Helicobacter pylori* cells were cultured with human gastric carcinoma cells. *Vibrio cholerae* and *Borrelia burgdorferi* were grown according to conditions in (Briegel *et al*., 2009; Briegel *et al*., 2016). *E. coli* were grown according to conditions in (Briegel *et al*., 2013; Briegel *et al*., 2012). *Caulobacter crescentus* were grown according to conditions in (Briegel *et al*., 2011). Prosthecobacters were all grown according to conditions in (Pilhofer *et al*., 2011). *Hyphomonas neptunium* was grown according to conditions in (Cserti *et al*., 2017).

In all cases, samples of cells in growth medium were mixed with BSA-treated 10 nm colloidal gold fiducials (Sigma), applied to glow-discharged EM grids (Quantifoil), and plunge-frozen in a liquid ethane-propane mixture (Tivol *et al.*, 2008). Grids were maintained at liquid nitrogen temperature throughout storage, transfer, and imaging.

*Electron cryotomography*

The references to growing conditions above also provide specific data collection settings. Generally, plunge-frozen samples were imaged using either a Polara or Titan Krios 300 kV FEG transmission electron microscope (FEI Company) equipped with an energy filter (Gatan). Images were recorded using either a lens-coupled 4k x 4k UltraCam CCD (Gatan) or a K2 Summit direct electron detector (Gatan). Tilt-series were recorded from -60° to +60° in 1-2° increments, with defoci of ~6-12 µm and a cumulative dose of ~100-200 $e^-/Å^2$. Tilt-series were acquired automatically using either Leginon (Suloway *et al.*, 2009) or UCSF Tomography (Zheng *et al.*, 2007) software. Tomographic reconstructions were calculated using either the IMOD software package (Kremer *et al.*, 1996) or Raptor (Amat *et al.*, 2008). 3D segmentations and movies were produced with IMOD (Kremer *et al.*, 1996). Subtomogram averages were calculated using PEET software (Nicastro *et al.*, 2006).

## ACKNOWLEDGMENTS

The authors would like to thank our collaborators who provided strains for imaging: Andrew Camilli (*Streptococcus pneumoniae*), Eric Matson (strain JT5), Gladys Alexandre (*Azospirillum brasilense* mutants), Lotte Søgaard-Andersen, Simon Ringgaard and Matthew K. Waldor (*Vibrio*

*cholerae* wild type and mutants), Michael Marletta (*Shewanella putrefaciens*), and Gordon Cannon and Sabine Heinhorst (*Halothiobacillus neapolitanus and Thiomonas intermedia*). We also thank members of the Jensen lab for helpful discussions.

## COMPETING INTERESTS

No competing interests declared.

## AUTHOR CONTRIBUTIONS

Conceptualization: M.J.D. and G.J.J.; formal analysis and investigation: M.J.D., C.M.O., A.P., J.C., K.G., T.J., J.T., J.D., Y.P., A.K., A.I.J., M.P., S.C., E.I.T., Y.-W.C., A.B., J.S., Z.L., P.S., C.V.I., B.A.S., A.W.M.; writing – original draft preparation: M.J.D. and C.M.O.; writing – review and editing: M.J.D., C.M.O., G.J.J.; funding acquisition: M.J.D. and G.J.J.; resources: G.J.J.; supervision: M.J.D. and G.J.J.

## FUNDING

This work was supported by the Hampshire College Dr. Lucy fund and the Collaborative Modeling Center, the NIH grant R01 AI27401 to GJJ, the Beckman Institute at Caltech, the Gordon and Betty Moore Foundation, the Human Frontier Science Program, the Howard Hughes Medical Institute, and the John Templeton Foundation as part of the Boundaries of Life project. The opinions expressed in this publication are those of the authors and do not necessarily reflect the views of the John Templeton Foundation.

## REFERENCES


Abrusci, P., M. Vergara-Irigaray, S. Johnson, M.D. Beeby, D.R. Hendrixson, P. Roversi, M.E. Friede, J.E. Deane, G.J. Jensen, C.M. Tang & S.M. Lea, (2013) Architecture of the major component of the type III secretion system export apparatus. *Nat Struct Mol Biol* **20**: 99-104.

Amat, F., F. Moussavi, L.R. Comolli, G. Elidan, K.H. Downing & M. Horowitz, (2008) Markov random field based automatic image alignment for electron tomography. *J Struct Biol* **161**: 260-275.

Aylett, C.H., Q. Wang, K.A. Michie, L.A. Amos & J. Lowe, (2010) Filament structure of bacterial tubulin homologue TubZ. *Proc Natl Acad Sci U S A* **107**: 19766-19771.

Barry, R.M. & Z. Gitai, (2011) Self-assembling enzymes and the origins of the cytoskeleton. *Current opinion in microbiology* **14**: 704-711.

Basler, M., M. Pilhofer, G.P. Henderson, G.J. Jensen & J.J. Mekalanos, (2012) Type VI secretion requires a dynamic contractile phage tail-like structure. *Nature* **483**: 182-186.

Beeby, M., J.C. Gumbart, B. Roux & G.J. Jensen, (2013) Architecture and assembly of the Gram-positive cell wall. *Mol Microbiol* **88**: 664-672.

Bharat, T.A., G.N. Murshudov, C. Sachse & J. Lowe, (2015) Structures of actin-like ParM filaments show architecture of plasmid-segregating spindles. *Nature* **523**: 106-110.

Bible, A., M.H. Russell & G. Alexandre, (2012) The *Azospirillum brasilense* Che1 chemotaxis pathway controls swimming velocity, which affects transient cell-to-cell clumping. *J Bacteriol* **194**: 3343-3355.

Bible, A.N., G.K. Khalsa-Moyers, T. Mukherjee, C.S. Green, P. Mishra, A. Purcell, A. Aksenova, G.B. Hurst & G. Alexandre, (2015) Metabolic adaptations of *Azospirillum brasilense* to oxygen stress by cell-to-cell clumping and flocculation. *Appl Environ Microbiol* **81**: 8346-8357.

Briegel, A., H.J. Ding, Z. Li, J. Werner, Z. Gitai, D.P. Dias, R.B. Jensen & G.J. Jensen, (2008) Location and architecture of the *Caulobacter crescentus* chemoreceptor array. *Mol Microbiol* **69**: 30-41.

Briegel, A., D.R. Ortega, E.I. Tocheva, K. Wuichet, Z. Li, S. Chen, A. Müller, C.V. Iancu, G.E. Murphy, M.J. Dobro, I.B. Zhulin & G.J. Jensen, (2009) Universal architecture of bacterial chemoreceptor arrays. *Proc Natl Acad Sci U S A* ***106****: 17181-17186.*

Briegel, A., M. Beeby, M. Thanbichler & G.J. Jensen, (2011) Activated chemoreceptor arrays remain intact and hexagonally packed. *Mol Microbiol* **82**: 748-757.

402 Briegel, A., X. Li, A.M. Bilwes, K.T. Hughes, G.J. Jensen & B.R. Crane, (2012) Bacterial
403 chemoreceptor arrays are hexagonally packed trimers of receptor dimers networked by
404 rings of kinase and coupling proteins. *Proc Natl Acad Sci U S A* **109**: 3766-3771.

405 Briegel, A., P. Ames, J.C. Gumbart, C.M Oikonomou, J.S. Parkinson &G.J. Jensen, (2013) The
406 mobility of two kinase domains in the *Escherichia coli* chemoreceptor array varies with
407 signalling state. *Mol Microbiol* **89**: 831-841.

408 Briegel, A., D.R. Ortega, P. Mann, A. Kjær, S. Ringgaard & G.J Jensen, (2016) Chemotaxis
409 cluster 1 proteins form cytoplasmic arrays in *Vibrio cholerae* and are stabilized by a
410 double signaling domain receptor DosM. *Proc Natl Acad Sci U S A* ***113****: 10412-10417.*

411 Cameron, D.E., J.M. Urbach & J.J. Mekalanos, (2008) A defined transposon mutant library and
412 its use in identifying motility genes in *Vibrio cholerae*. *Proc Natl Acad Sci U S A* **105**:
413 8736-8741.

414 Chang, Y.W., S. Chen, E.I. Tocheva, A. Treuner-Lange, S. Lobach, L. Sogaard-Andersen & G.J.
415 Jensen, (2014) Correlated cryogenic photoactivated localization microscopy and cryo-
416 electron tomography. *Nature methods* **11**: 737-739.

417 Chang, Y.W., L.A. Rettberg, A. Treuner-Lange, J. Iwasa, L. Sogaard-Andersen & G.J. Jensen,
418 (2016) Architecture of the type IVa pilus machine. *Science* **351**: aad2001.

419 Chen, S., M. Beeby, G.E. Murphy, J.R. Leadbetter, D.R. Hendrixson, A. Briegel, Z. Li, J. Shi,
420 E.I. Tocheva, A. Muller, M.J. Dobro & G.J. Jensen, (2011) Structural diversity of
421 bacterial flagellar motors. *EMBO* **30**: 2972-2981.

422 Cserti E., S. Rosskopf, Y-W. Chang, S. Eisheuer, L. Selter, J. Shi, C. Regh, U. Koert, G.J. Jensen
423 & M. Thanbichler, (2017) Dynamics of the peptidoglycan biosynthetic machinery in the
424 stalked budding bacterium *Hyphomonas neptunium*. *Mol Microbiol* **103**: 875-895.

425 De Troch, P. & J. Vanderleyden, (1996) Surface Properties and Motility of Rhizobium and
426 Azospirillum in Relation to Plant Root Attachment. *Microb Ecol* **32**: 149-169.

427 Ding, H.J., C.M. Oikonomou & G.J. Jensen, (2015) The Caltech Tomography Database and
428 Automatic Processing Pipeline. *J Struct Biol* **192**: 279-286.

429 Dueholm, M.S., M. Albertsen, D. Otzen & P.H. Nielsen, (2012) Curli functional amyloid
430 systems are phylogenetically widespread and display large diversity in operon and
431 protein structure. *PLoS One* **7**: e51274.

432 Ebersbach, G., A. Briegel, G.J. Jensen & C. Jacobs-Wagner, (2008) A self-associating protein
433 critical for chromosome attachment, division, and polar organization in Caulobacter. *Cell*
434 **134**: 956-968.

435 Egelman, E.H. & A. Stasiak, (1986) Structure of helical RecA-DNA complexes. Complexes
436 formed in the presence of ATP-gamma-S or ATP. *J Mol Biol* **191**: 677-697.

437 Epstein, E.A., M.A. Reizian & M.R. Chapman, (2009) Spatial clustering of the curlin secretion
438 lipoprotein requires curli fiber assembly. *J Bacteriol* **191**: 608-615.

439 Gan, L., S. Chen & G.J. Jensen, (2008) Molecular organization of Gram-negative peptidoglycan.
440 *Proc Natl Acad Sci U S A* **105**: 18953-18957.

441 Gonin, M., E.M. Quardokus, D. O'Donnol, J. Maddock & Y.V. Brun, (2000) Regulation of stalk
442 elongation by phosphate in *Caulobacter crescentus*. *J Bacteriol* **182**: 337-347.

443 Guerrero-Ferreira, R.C., P.H. Viollier, B. Ely, J.S. Poindexter, M. Georgieva, G.J. Jensen & E.R.
444 Wright, (2011) Alternative mechanism for bacteriophage adsorption to the motile
445 bacterium *Caulobacter crescentus*. *Proc Natl Acad Sci U S A* **108**: 9963-9968.

446 Iancu, C.V., H.J. Ding, D.M. Morris, D.P. Dias, A.D. Gonzales, A. Martino & G.J. Jensen,
447 (2007) The structure of isolated *Synechococcus* strain WH8102 carboxysomes as
448 revealed by electron cryotomography. *J Mol Biol* **372**: 764-773.

449 Ingerson-Mahar, M., A. Briegel, J.N. Werner, G.J. Jensen & Z. Gitai, (2010) The metabolic
450 enzyme CTP synthase forms cytoskeletal filaments. *Nature cell biology* **12**: 739-746.

451 Jones, L.J., R. Carballido-Lopez & J. Errington, (2001) Control of cell shape in bacteria: helical,
452 actin-like filaments in *Bacillus subtilis*. *Cell* **104**: 913-922.

453 Komeili, A., Z. Li, D.K. Newman & G.J. Jensen, (2006) Magnetosomes are cell membrane
454 invaginations organized by the actin-like protein MamK. *Science* **311**: 242-245.

455 Koster, A.J., R. Grimm, D. Typke, R. Hegerl, A. Stoschek, J. Walz & W. Baumeister, (1997)
456 Perspectives of molecular and cellular electron tomography. *J Struct Biol* **120**: 276-308.

457 Kremer, J.R., D.N. Mastronarde & J.R. McIntosh, (1996) Computer visualization of three-
458 dimensional image data using IMOD. *J Struct Biol* **116**: 71-76.

459 Kuhn, J., A. Briegel, E. Morschel, J. Kahnt, K. Leser, S. Wick, G.J. Jensen & M. Thanbichler,
460 (2010) Bactofilins, a ubiquitous class of cytoskeletal proteins mediating polar localization
461 of a cell wall synthase in *Caulobacter crescentus*. *EMBO* **29**: 327-339.

462 Laurenceau, R., P.V. Krasteva, A. Diallo, S. Ouarti, M. Duchateau, C. Malosse, J. Chamot-
463 Rooke & R. Fronzes, (2015) Conserved *Streptococcus pneumoniae* spirosomes suggest a
464 single type of transformation pilus in competence. *PLoS Pathog* **11**: e1004835.

465 Li, Z., M.J. Trimble, Y.V. Brun & G.J. Jensen, (2007) The structure of FtsZ filaments in vivo
466 suggests a force-generating role in cell division. *EMBO* **26**: 4694-4708.

467 Lim, C.J., S.Y. Lee, J. Teramoto, A. Ishihama & J. Yan, (2013) The nucleoid-associated protein
468 Dan organizes chromosomal DNA through rigid nucleoprotein filament formation in *E.*
469 *coli* during anoxia. *Nucleic Acids Res* **41**: 746-753.

Lonhienne, T.G., E. Sagulenko, R.I. Webb, K.C. Lee, J. Franke, D.P. Devos, A. Nouwens, B.J. Carroll & J.A. Fuerst, (2010) Endocytosis-like protein uptake in the bacterium *Gemmata obscuriglobus*. *Proc Natl Acad Sci U S A* **107**: 12883-12888.

Makarova, K.S. & E.V. Koonin, (2010) Two new families of the FtsZ-tubulin protein superfamily implicated in membrane remodeling in diverse bacteria and archaea. *Biol Direct* **5**: 33.

Matayoshi, S., H. Oda & G. Sarwar, (1989) Relationship between the production of spirosomes and anaerobic glycolysis activity in *Escherichia coli* B. *J Gen Microbiol* **135**: 525-529.

Mizuno, N., M. Dramicanin, M. Mizuuchi, J. Adam, Y. Wang, Y.W. Han, W. Yang, A.C. Steven, K. Mizuuchi & S. Ramon-Maiques, (2013) MuB is an AAA+ ATPase that forms helical filaments to control target selection for DNA transposition. *Proc Natl Acad Sci U S A* **110**: E2441-2450.

Moissl, C., R. Rachel, A. Briegel, H. Engelhardt & R. Huber, (2005) The unique structure of archaeal 'hami', highly complex cell appendages with nano-grappling hooks. *Mol Microbiol* **56**: 361-370.

Mukherjee, T., D. Kumar, N. Burriss, Z. Xie & G. Alexandre, (2016) *Azospirillum brasilense* chemotaxis depends on two signaling pathways regulating distinct motility parameters. *J Bacteriol* **198**: 1764-1772.

Muller, A., M. Beeby, A.W. McDowall, J. Chow, G.J. Jensen & W.M. Clemons, Jr., (2014) Ultrastructure and complex polar architecture of the human pathogen *Campylobacter jejuni*. *MicrobiologyOpen* **3**: 702-710.

Murphy, G.E., J.R. Leadbetter & G.J. Jensen, (2006) In situ structure of the complete *Treponema primitia* flagellar motor. *Nature* **442**: 1062-1064.

Murphy, G.E., E.G. Matson, J.R. Leadbetter, H.C. Berg & G.J. Jensen, (2008) Novel ultrastructures of *Treponema primitia* and their implications for motility. *Mol Microbiol* **67**: 1184-1195.

Nicastro, D., C. Schwartz, J. Pierson, R. Gaudette, M.E. Porter & J.R. McIntosh, (2006) The molecular architecture of axonemes revealed by cryoelectron tomography. *Science* **313**: 944-948.

Oikonomou, C.M. & G.J. Jensen, (2016) A new view into prokaryotic cell biology from electron cryotomography. *Nat Rev Microbiol* **14**: 205-220.

Pilhofer, M., M.S. Ladinsky, A.W. McDowall & G.J. Jensen, (2010) Bacterial TEM: new insights from cryo-microscopy. *Methods Cell Biol* **96**: 21-45.

Pilhofer, M., M.S. Ladinsky, A.W. McDowall, G. Petroni & G.J. Jensen, (2011) Microtubules in bacteria: Ancient tubulins build a five-protofilament homolog of the eukaryotic cytoskeleton. *PLoS Biol* **9**: e1001213.

506 Pommier, Y., J.M. Covey, D. Kerrigan, J. Markovits & R. Pham, (1987) DNA unwinding and
507 inhibition of mouse leukemia L1210 DNA topoisomerase I by intercalators. *Nucleic*
508 *Acids Res* **15**: 6713-6731.

509 Ruska, E., (1987) Nobel lecture. The development of the electron microscope and of electron
510 microscopy. *Biosci Rep* **7**: 607-629.

511 Santarella-Mellwig, R., J. Franke, A. Jaedicke, M. Gorjanacz, U. Bauer, A. Budd, I.W. Mattaj &
512 D.P. Devos, (2010) The compartmentalized bacteria of the Planctomycetes-
513 Verrucomicrobia-Chlamydiae superphylum have membrane coat-like proteins. *PLoS*
514 *biology* **8**: e1000281.

515 Scheffel, A., M. Gruska, D. Faivre, A. Linaroudis, J.M. Plitzko & D. Schuler, (2006) An acidic
516 protein aligns magnetosomes along a filamentous structure in magnetotactic bacteria.
517 *Nature* **440**: 110-114.

518 Schlimpert, S., E.A. Klein, A. Briegel, V. Hughes, J. Kahnt, K. Bolte, U.G. Maier, Y.V. Brun,
519 G.J. Jensen, Z. Gitai & M. Thanbichler, (2012) General protein diffusion barriers create
520 compartments within bacterial cells. *Cell* **151**: 1270-1282.

521 Shih, Y.L., T. Le & L. Rothfield, (2003) Division site selection in *Escherichia coli* involves
522 dynamic redistribution of Min proteins within coiled structures that extend between the
523 two cell poles. *Proc Natl Acad Sci U S A* **100**: 7865-7870.

524 Staley, J.T., J.A. Bont & K. Jonge, (1976) *Prosthecobacter fusiformis* nov. gen. et ap., the
525 fusiform caulobacter. *Antonie Van Leeuwenhoek* **42**: 333-342.

526 Steenhoudt, O. & J. Vanderleyden, (2000) Azospirillum, a free-living nitrogen-fixing bacterium
527 closely associated with grasses: genetic, biochemical and ecological aspects. *FEMS*
528 *Microbiol Rev* **24**: 487-506.

529 Suloway, C., J. Shi, A. Cheng, J. Pulokas, B. Carragher, C.S. Potter, S.Q. Zheng, D.A. Agard &
530 G.J. Jensen, (2009) Fully automated, sequential tilt-series acquisition with Leginon. *J*
531 *Struct Biol* **167**: 11-18.

532 Swulius, M.T., S. Chen, H. Jane Ding, Z. Li, A. Briegel, M. Pilhofer, E.I. Tocheva, S.R.
533 Lybarger, T.L. Johnson, M. Sandkvist & G.J. Jensen, (2011) Long helical filaments are
534 not seen encircling cells in electron cryotomograms of rod-shaped bacteria. *Biochemical*
535 *and biophysical research communications* **407**: 650-655.

536 Swulius, M.T. & G.J. Jensen, (2012) The helical MreB cytoskeleton in *Escherichia coli*
537 MC1000/pLE7 is an artifact of the N-Terminal yellow fluorescent protein tag. *J Bacteriol*
538 **194**: 6382-6386.

539 Szwedziak, P., Q. Wang, T.A. Bharat, M. Tsim & J. Lowe, (2014) Architecture of the ring
540 formed by the tubulin homologue FtsZ in bacterial cell division. *eLife* **4**.

Teramoto, J., S.H. Yoshimura, K. Takeyasu & A. Ishihama, (2010) A novel nucleoid protein of *Escherichia coli* induced under anaerobiotic growth conditions. *Nucleic Acids Res* **38**: 3605-3618.

Tivol, W.F., A. Briegel & G.J. Jensen, (2008) An improved cryogen for plunge freezing. *Microscopy and Microanalysis* **14**: 375-379.

Tocheva, E.I., E.G. Matson, D.M. Morris, F. Moussavi, J.R. Leadbetter & G.J. Jensen, (2011) Peptidoglycan remodeling and conversion of an inner membrane into an outer membrane during sporulation. *Cell* **146**: 799-812.

Van Gerven, N., R.D. Klein, S.J. Hultgren & H. Remaut, (2015) Bacterial amyloid formation: Structural insights into curli biogensis. *Trends Microbiol* **23**: 693-706.

Wagner, J.K., Setayeshgar, S., Sharon, L.A., J.P. Reilly & Y.V. Brun, (2006) A nutrient uptake role for bacterial cell envelope extensions. *Proc Natl Acad sci U S A* **103**: 11772-11777.

Weiner, R.M., M. Melick, K. O'Neill & E. Quintero, (2000) *Hyphomonas adhaerens sp. nov.*, *Hyphomonas johnsonii sp. nov.* and *Hyphomonas rosenbergii sp. nov.*, marine budding and prosthecate bacteria. *Int J Syst Evol Microbiol* **50 Pt 2**: 459-469.

Wolf, S.G., D. Frenkiel, T. Arad, S.E. Finkel, R. Kolter & A. Minsky, (1999) DNA protection by stress-induced biocrystallization. *Nature* **400**: 83-85.

Zerfas, P.M., M. Kessel, E.J. Quintero & R.M. Weiner, (1997) Fine-structure evidence for cell membrane partitioning of the nucleoid and cytoplasm during bud formation in Hyphomonas species. *J Bacteriol* **179**: 148-156.

Zheng, S.Q., B. Keszthelyi, E. Branlund, J.M. Lyle, M.B. Braunfeld, J.W. Sedat & D.A. Agard, (2007) UCSF tomography: an integrated software suite for real-time electron microscopic tomographic data collection, alignment, and reconstruction. *J Struct Biol* **157**: 138-147.

## FIGURE LEGENDS

**Figure 1. Novel *Prosthecobacter debontii* appendages.** Multiple external appendages (arrowheads) were observed by ECT on *P. debontii* prosthecae **(A)**. A central tomographic slice is shown, with a single appendage enlarged in the inset. Subtomogram averaging revealed the structure in more detail. Side (above) and top (below) views in **(B)** show the characteristic disc-like densities and the five legs attaching to the cell surface. The red box shows which view was

572 used to rotate the image 90° for the bottom image. **(C)** shows a 3D isosurface of the average,
573 seen from the side and top (inset). Scale bars 50 nm in **(A)** and 20 nm in inset.
574
575 **Figure 2. Novel *Azospirillum brasilense* hooks.** Many hook-like structures were observed on
576 the surface of *A. brasilense* cells. A central tomographic slice is shown, with arrowheads
577 indicating hooks. A single hook is shown enlarged at right. Scale bar 50 nm.
578
579 **Figure 3. Strain JT5 fimbriae.** Examples are shown from two cells of strain JT5 (related to
580 the Dysgonomonas genus) exhibiting abundant fimbrae at the cell pole. **(A)** shows a central
581 slice revealing overall cell morphology and **(B-D)** show slices at progressive z-heights through
582 a cryotomogram of a cell of strain JT5 (related to the *Dysgonomonas* genus). Abundant
583 fimbriae can be seen at the cell pole. Scale bars 100 nm.
584
585 **Figure 4. Novel *Vibrio cholerae* nanospheres.** Clusters of "nanospheres" were observed in
586 two cryotomograms of *V. cholerae* cells (central slices shown in **A** and **C**). "N" indicates
587 nanospheres; "A" indicates associated filament array. **(B)** shows a segmentation of the cluster
588 seen in **(A)**, with outer and inner membranes in magenta and cyan, respectively, and
589 nanospheres in green. A clipping plane cuts through the 3D segmentation revealing the thick
590 walls and hollow centers of the nanospheres. Scale bars 100 nm.
591
592 **Figure 5. Filament bundles, arrays, and chains.** *Hyphomonas neptunium* division stalks
593 contained helical bundles (**A**) that straightened when cells were treated with ethidium bromide
594 (**B**). The right side of panel (**A**) shows a 3D segmentation of the helical bundle, with side and

595 top views of subtomogram averaged insets. Labeled dimensions are in nanometers. (**C**) Large
596 filament bundles in *Helicobacter pylori*. (**D**) A long mesh-like filament array in *Vibrio*
597 *cholerae*, with segmentation at right. (**E**) A more typical *V. cholerae* filament array. Filament
598 arrays in *Thiomonas intermedia* (**F**), *Hyphomonas neptunium* (**G**) *Hylemonella gracilis* (**H**),
599 *Halothiobacillus neapolitanus* c2 (**I**), and *Mycobacterium smegmatis* (**J**). (**K**) A chain in
600 *Prosthecobacter vanneervenii*. (**L-M**) Filament arrays in *Prosthecobacter debontii*. (**N**) A
601 filament array in a starved *Campylobacter jejuni* cell. Scale bars 100 nm (A-B, D-J, L-N) and
602 50 nm (C,K).
603
604 **Figure 6. Single and paired filaments.** Tomographic slices showing paired filaments in
605 *Campylobacter jejuni* (**A**), and *Thiomicrospira crunogena* (**B**), and membrane-aligned filaments
606 in *Shewanella putrefaciens* (**C**), *Prosthecobacter debontii* ***(D)***, and *Prosthecobacter fluviatilis*
607 (**E**, red arrow shows filament just under the inner membrane). Scale bars 100 nm (A-D) and 50
608 nm (E).
609
610 **Figure 7. Tubes and rings.** Tubes observed in *Thiomicrospira crunogena* (**A**),
611 *Halothiobacillus neapolitanus c2* (**B**), *Bdellovibrio bacteriovorus* (**C**), *Thiomonas intermedia*
612 (**D**), and *Hyphomonas neptunium* (**E**). In each panel, tomographic slices show a side view
613 (above), and a top view (bottom). (**F**) An array of rings observed in *Helicobacter pylori*. Scale
614 bars 10 nm (A,C,E), 20 nm (B,D), and 100 nm (F).
615
616 **Figure 8. Round and horseshoe-shaped vesicles.** Tomographic slices showing examples of
617 round vesicles in *Escherichia coli* (**A**, segmentation shown at right), *Helicobacter pylori* (**B**),

618 *Helicobacter hepaticus* (**C**), *Myxococcus xanthus* (**D**), *Caulobacter crescentus* (**E**), and
619 *Myxococcus xanthus* overexpressing PilP-sfGFP (**F**). Examples of horseshoe-shaped vesicles in
620 *Ralstonia eutropha* (**G**) and *Prosthecobacter fluviatilis* (**H**), with 3D segmentations shown at
621 right. In the segmentation in (A), outer and inner membranes are in magenta and cyan,
622 respectively, and vesicles in green. Scale bars 50 nm.
623
624 **Figure 9. Flattened and nested vesicles.** Examples of flattened vesicles in *Thiomonas*
625 *intermedia* (**A**), *Caulobacter crescentus* (**B-E**) and *Prosthecobacter debontii* (**F**). Note storage
626 granules in (E and F), shown in orange in the segmentation in (E). Examples of nested vesicles
627 in *Serpens flexibilis* (**G**), *Caulobacter crescentus* (**H**), *Borrelia burgdorferi* (**I**), *Vibrio cholerae*
628 (**J**), *Caulobacter crescentus* with segmentation (**K**), and strain JT5 (**L**). Inset in (L) shows an
629 enlargement of central vesicle, and a 3D segmentation of the visible portion of the cell is shown
630 below. In segmentations, outer and inner membranes are shown in magenta and cyan,
631 respectively, and vesicles in green. Scale bars 50 nm.
632
633 **Figure 10. Periplasmic vesicles.** Examples of periplasmic vesicles in *Caulobacter crescentus*
634 (**A**), *Helicobacter pylori* (**B**), *Brucella abortus* (**C**), *Thiomonas intermedia* (**D**), *Hyphomonas*
635 *neptunium* (**E**), *Myxococcus xanthus* (**F**), and *Halothiobacillus neapolitanus* c2 (**G**). In each
636 panel, a central tomographic slice is shown, as well as a segmentation with outer and inner
637 membranes in magenta and cyan, respectively, and vesicles in green. Scale bars 50 nm (A-F)
638 and 100 nm (G).
639
640

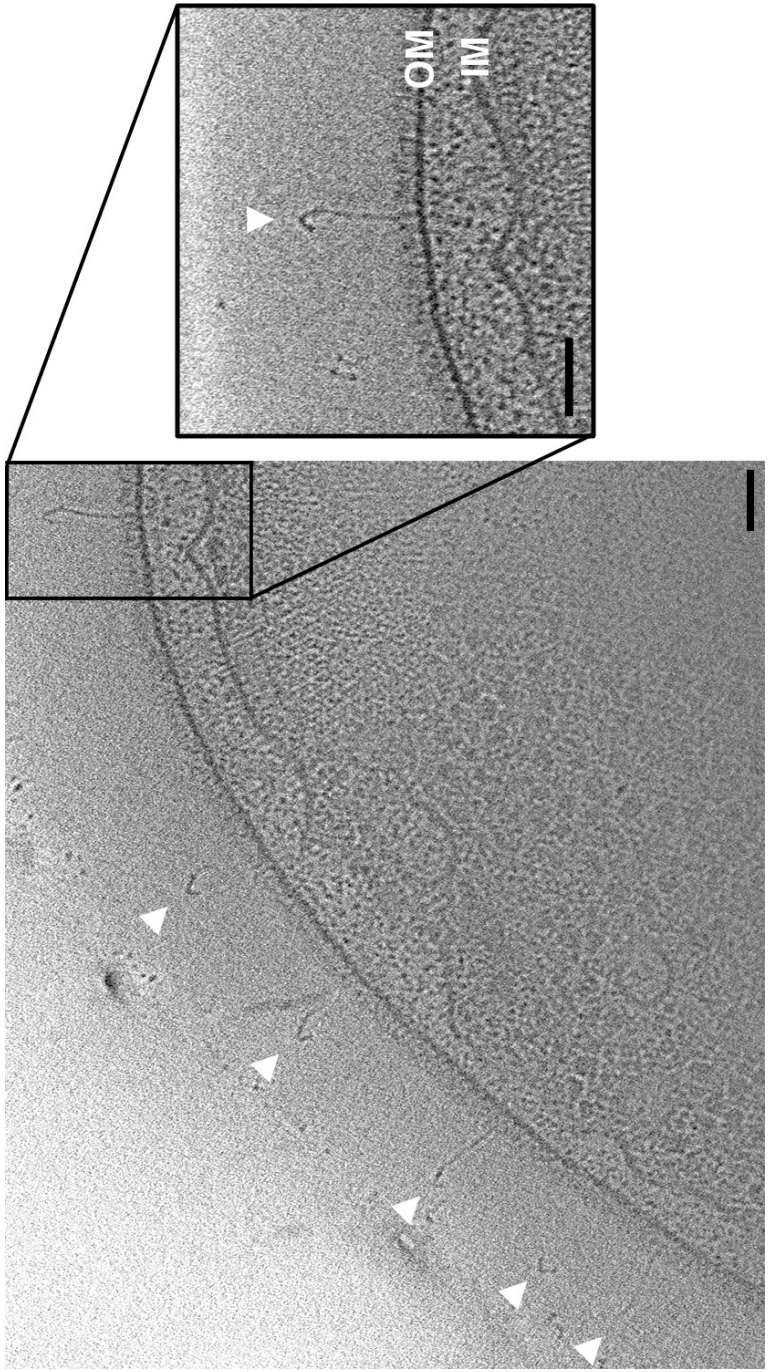

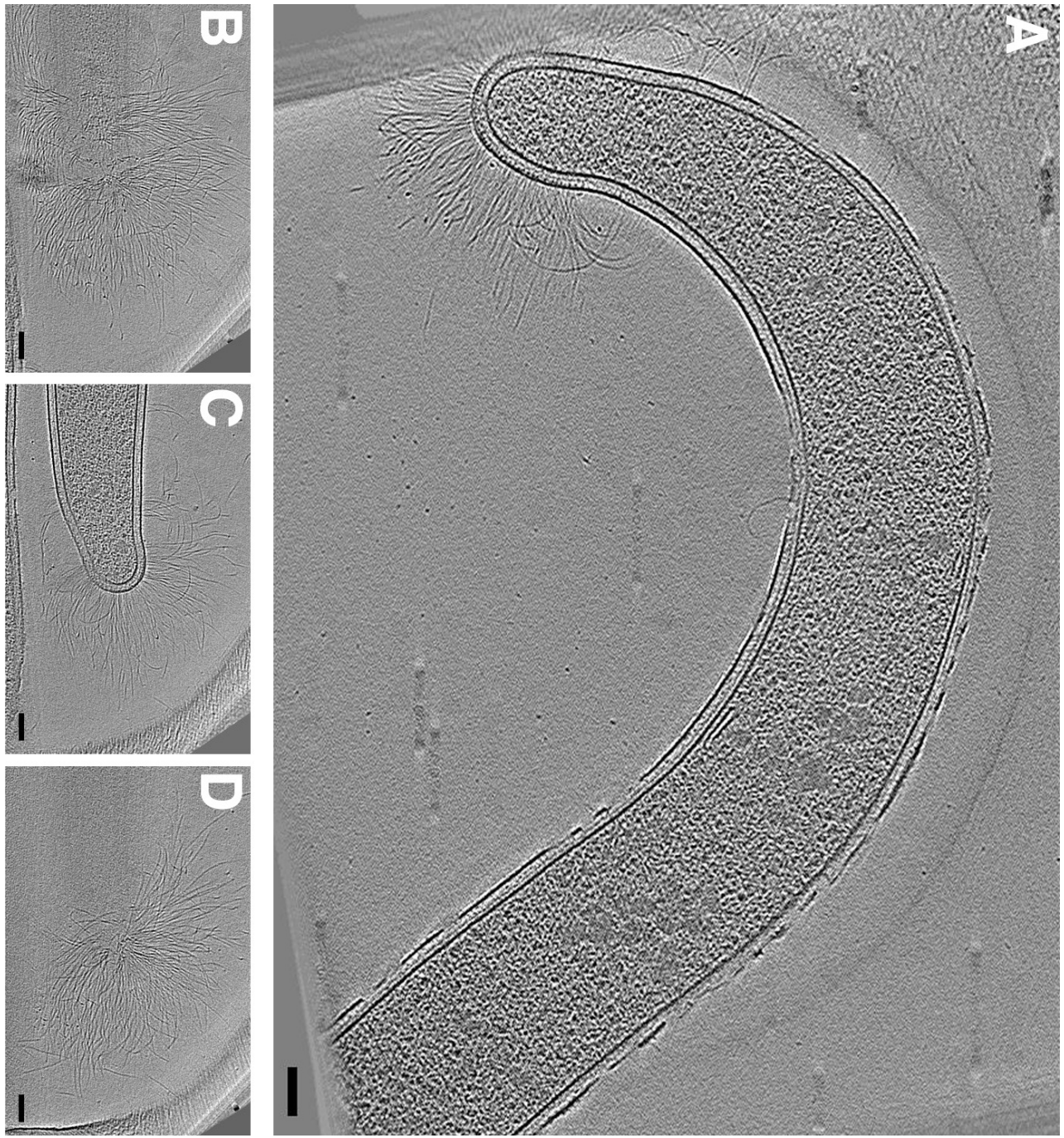

Journal of Bacteriology

JB

Journal of Bacteriology

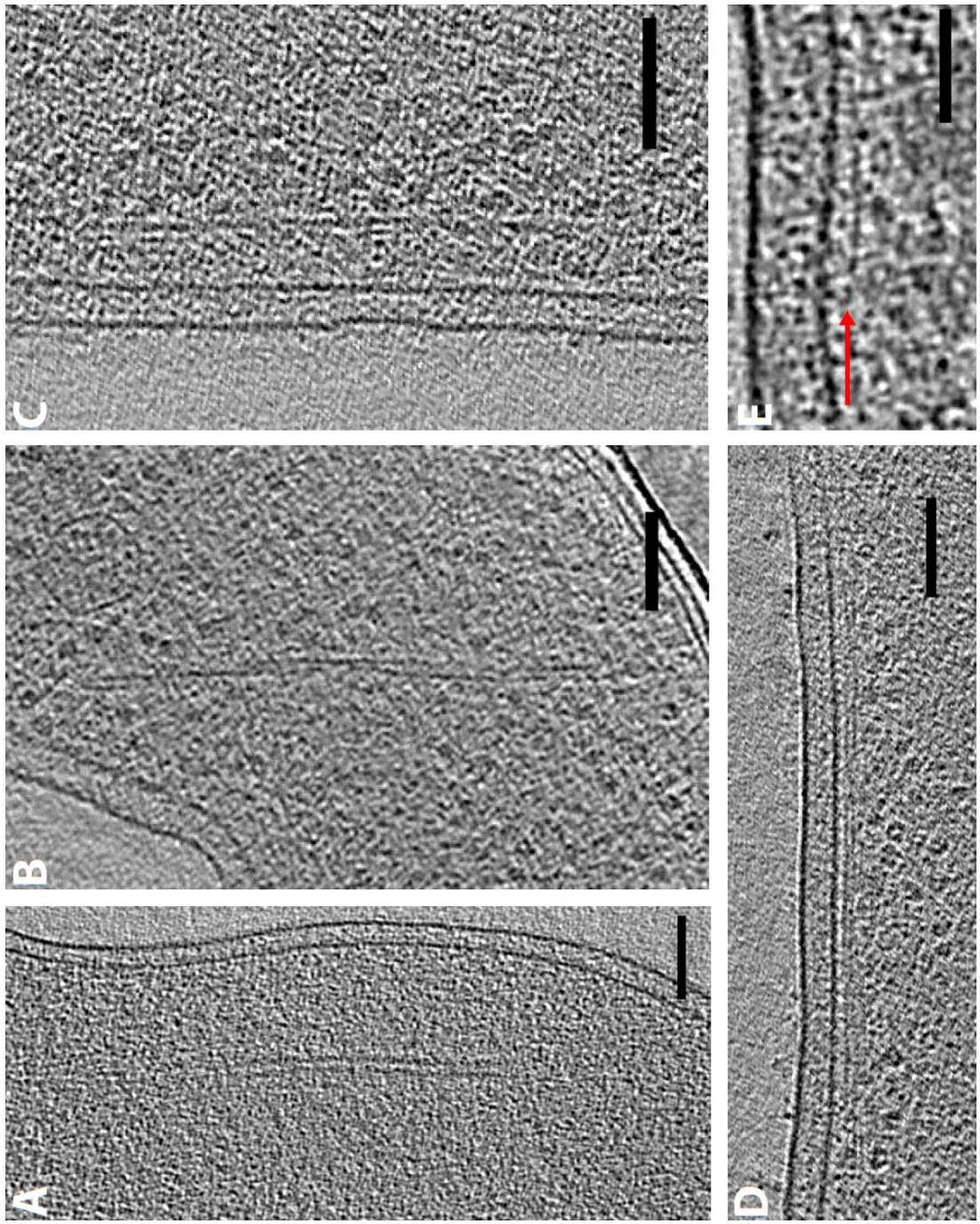

Journal of Bacteriology

JB

Journal of Bacteriology